Soft Matter

PAPER

View Article Online
View Journal | View Issue

Cite this: *Soft Matter*, 2025, **21**, 8849

Resolving the mechanical response of liquid crystal elastomers – semi-soft elastic or auxetic

Thomas Raistrick, *† Matthew Reynolds, † Emily J. Cooper, Jordan Hobbs, Victor Reshetnyak and Helen F. Gleeson

Liquid crystal elastomers (LCEs) display one of two distinct behaviours under deformations perpendicular to the nematic director: semi-soft elastic (SSE) or biaxial auxetic responses. The physical reason why an LCE should show one rather than the other response has so far remained elusive. Furthermore, while these responses have been observed individually, they have yet to be reported simultaneously or in chemically similar LCEs. Here, a series of monodomain side-chain LCEs with varying cross-link density is studied. At higher cross-link densities, the samples display a clear auxetic (negative Poisson's ratio) response, while at lower cross-link densities, the behaviour is consistent with the SSE response. At intermediate cross-link densities, the behaviour includes both auxetic and SSE natures. A theoretical framework is established from a modified Maier–Saupe model which quantifies the larger internal stresses in the higher cross-link density LCEs; a factor of ~3.3 greater internal stress is found between systems with a factor of 8 difference in cross-link density. We suggest that the internal field can, if sufficiently large, be a factor in causing the LCE to deform biaxially (and therefore auxetically), rather than uniaxially under strain. Using tensile measurements, cross-polarised microscopy and X-ray spectroscopy, we demonstrate that the deformation behaviour of these LCEs lies on a continuum and is a combination of the extent of the nematic ordering, robustness of nematic coupling, and relaxation dynamics. We show the importance of polymer dynamics in these systems, such that a reduction in the auxetic threshold occurs upon lowering strain rates or increasing temperature.

Received 1st July 2025,
Accepted 23rd October 2025

DOI: 10.1039/d5sm00677e

rsc.li/soft-matter-journal

Introduction

Liquid crystal elastomers (LCEs), consisting of a lightly cross-linked polymeric network containing mesogenic units, are a remarkable class of materials which display unique mechanical behaviours and responsiveness to external stimuli. Perhaps one of the most commonly known features associated with most LCEs is their ability to display a 'semi-soft elastic' (SSE) response to deformations perpendicular to their nematic director.[1,2] In the SSE response, there is little-to-no elastic cost of deformation due to the continuous in-plane (uniaxial) rotation of the director to align with the strain axis. The 'semi' in semi-soft elasticity is due to the observation of an initial 'high' elastic modulus region observed in the stress–strain curve which is followed by a much-reduced elastic modulus.[2,3] After the director has completely rotated to align with the direction of strain, there is a subsequent increase in the stress–strain response leading to the characteristic stress–strain curve (Fig. 1a) synonymous with semi-soft elasticity. In addition to the softened plateau region there is the observation of 'stripe domains' which are domains of counter rotating director angles running parallel to the strain direction.[1,4,5]

Yet another intriguing property of LCEs was reported in 2018, when it was discovered that, instead of displaying SSE behaviour, a certain class of LCEs exhibit an auxetic response.[6] 'Auxetics' are materials which have a negative Poisson's ratio, so that their thickness increases upon applied strain. Thus far, LCEs are the only known synthetic molecular auxetic materials and the auxetic response has been observed in a number of all acrylate LCEs[6–10] and a polybutadiene derived LCE.[11] The auxetic response has been shown to be related to a biaxial, rather than uniaxial, deformation and this alternative to the SSE response was previously referred to as a 'mechanical Fréedericksz transition' (MFT) because of the apparently discontinuous rotation of the director at a particular strain threshold.[6–8,12] In auxetic LCEs under strain, there is a reduction in the uniaxial order parameter and an emergence of biaxial order. The associated out-of-plane rotation of mesogenic units causes an increase in the thickness of auxetic LCEs in response to an applied strain;[7] a proposition supported by recent all-atomic molecular dynamic simulations.[13] The auxetic response in LCEs is volume-conserving and occurs at a

School of Physics and Astronomy, University of Leeds, LS2 9JT, UK.
E-mail: t.j.raistrick@leeds.ac.uk
† Joint first authorship contribution.

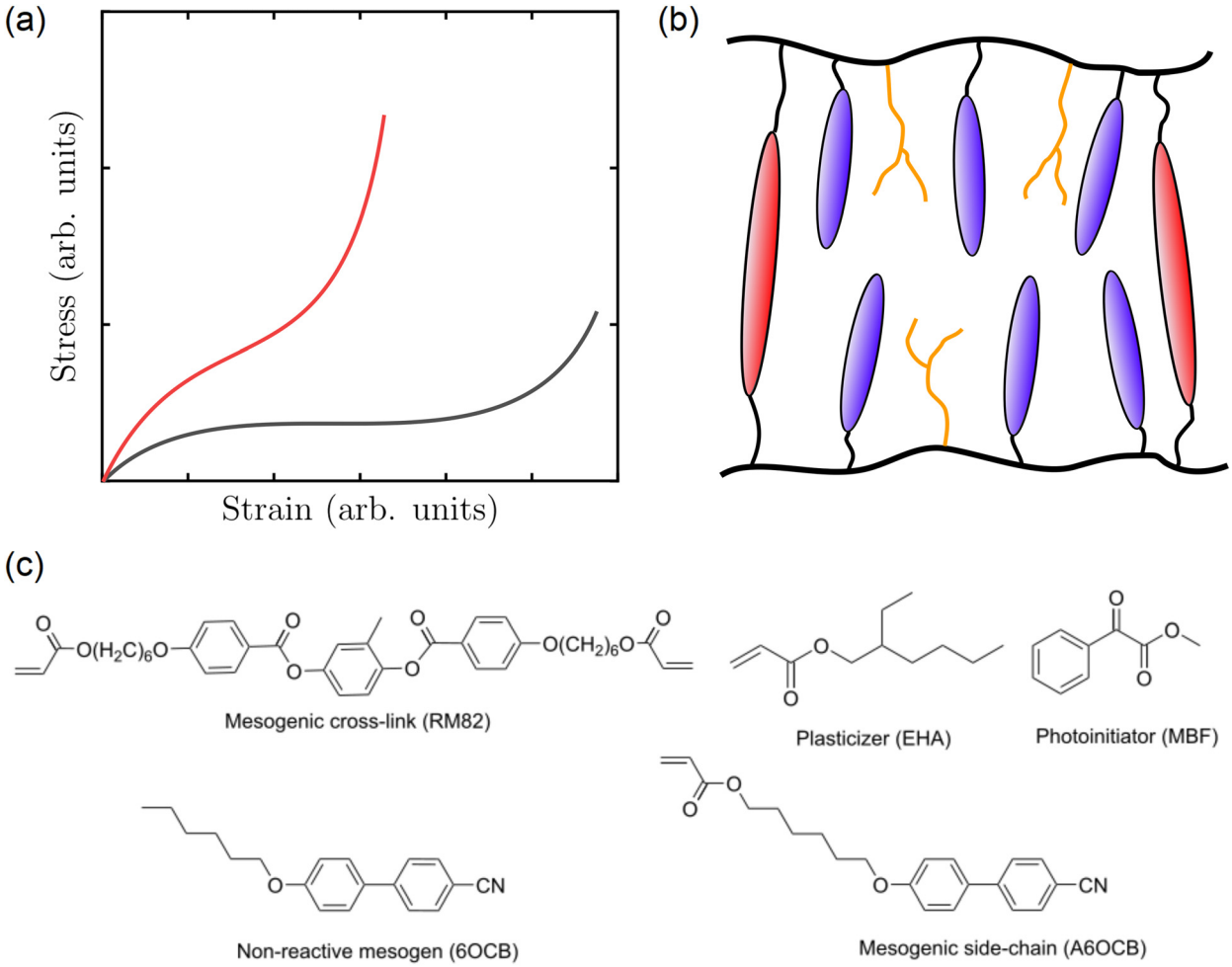

Fig. 1 (a) Schematic of the stress–strain response observed in an LCE displaying semi-soft elasticity (black) and a hyperelastic response observed in LCEs displaying auxeticity (red). (b) Schematic of the side-chain LCE network used in this work (red = RM82, blue = 6OCB, orange = EHA, black = acrylate backbone). (c) Chemical components of the precursor mixtures. 6-(4-Cyano-biphenyl-4′-yloxy)hexyl acrylate (A6OCB), 2-ethylhexyl acrylate (EHA), 1,4-bis-[4-(6-acryloyloxyhex-yloxy)benzoyloxy]-2-methylbenzene (RM82), 4-cyano-4′hexyloxybiphenyl (6OCB), and methyl benzoylformate (MBF).

molecular level, and these synthetic molecular auxetic materials are also the only known transparent auxetic materials.[6,14] Conversely, most other synthetic auxetic materials are 're-entrant' and are formed by creating porous structures in positive Poisson's ratio materials which are opaque due to their inherent porosity.[15,16] Under deformation the re-entrant structures unfold leading to a non-volume conserving auxetic response.

Whilst the mechanism for the auxetic response in LCEs is now well-understood to be related to biaxiality, the question remains as to why certain LCEs deform *via* the uniaxial SSE response while others deform *via* a biaxial auxetic deformation and thus a dichotomy of the two behaviours has been established. The stress–strain response of the auxetic LCEs is hyperelastic showing a similar 'S' shaped curve to that seen in semi-soft elasticity (Fig. 1a, black line), but its origins are quite distinct.[12] Predicting whether an LCE will exhibit SSE or auxetic behaviour is an outstanding puzzle which we address in this paper. We present experimental results for a family of LCEs which differ only in their cross-link density, and which display a uniaxial SSE or biaxial deformation, depending on the cross-link density. Understanding what causes the two different behaviours in such similar materials allows us to establish design rules for auxetic LCEs to tailor their response.

In addition to the differing mechanical responses of auxetic LCEs and SSE LCEs, there are differences in their thermal responses. The auxetic LCEs reported so far have shown no evidence of an obvious nematic-to-isotropic transition temperature, T_{NI}, when investigated *via* birefringence measurements, differential scanning calorimetry, or thermally driven shape changes.[12,17] Further, the phase of the elastomers can essentially be locked-in during polymerisation to produce chemically identical systems that are either nematic or, if polymerised at elevated temperatures, isotropic.[18,19] In comparison, other LCEs tend to display a T_{NI} which depends on both the mesogenic content[20] and the alignment technique.[19] This is an

important distinction between the two behaviours as the existence of an accessible isotropic reference state has been identified theoretically as a requirement for soft elasticity.[2,3,21] In discussing the nematic-to-isotropic transition in LCEs, it is important to note that in general there is no requirement for discontinuity at the transition (*i.e.* the transition does not have to be first order, unlike in low molar mass nematic systems) and instead there can be a continuous transition from the nematic to isotropic state.[22] Additionally, there is often residual order in the higher temperature phase which is commonly referred to as a para-nematic phase as opposed to a 'true' isotropic phase. This behaviour is known to be related to internal stresses, often discussed in the terms of an internal mechanical aligning field, which drives the transition from a first-order behaviour to a 'super-critical' behaviour.[22] A similar behaviour is observed in conventional (fluid) liquid crystal phases in the presence of large electric or magnetic fields.[23]

The presence of an internal mechanical field modifies both the thermal and mechanical response of LCEs. When an LCE is strained, the presence of an internal mechanical field requires that a threshold strain must be exceeded before a director rotation occurs and results in non-zero bend mode relaxations.[24,25] The internal mechanical field present means the C_5 elastic constant, associated with the energetic costs of strain in-plane of the director, is non-zero.[26] However, the Goldstone argument for soft elasticity requires that $C_5 = 0$.[21,27] Theoretically, it has been shown that semi-softness can still occur in the super-critical regime for small internal mechanical aligning fields through the existence of biaxial phases which spontaneously break symmetry upon deformation.[27–29] These theoretical arguments are explored here in the context of whether a SSE or auxetic response is observed in a specific LCE.

In this paper, a series of side chain liquid crystal elastomers with varying cross-link density, but an otherwise consistent chemical composition, are synthesised (Fig. 1b shows a schematic representation of the LCE network used herein). At a higher cross-link density, this particular system exhibits a clear auxetic response upon deformation,[6,8,9,17,30] however upon reducing the cross-link density, we show that the deformation behaviour is consistent with a classical SSE response. The transition between these two behaviours is also apparent in the intermediate cross-link regime, where both auxetic and SSE behaviours occur in a single material in specific regimes. The crossover from one deformation mode to the other gives insight into the structural and mechanical constraints needed to achieve an auxetic response in LCEs. A modified Maier–Saupe theory model is presented for the LCE (under no external strain) which can determine the relative scale of the internal mechanical stresses in the differently cross-linked LCEs from order parameter data. It is found that the higher cross-linked LCE has a significantly larger internal stress which we suggest in-part explains the difference between the SSE and auxetic response. Additionally, a dynamic dependence of the response is presented.

Experimental section

Sample preparation

Monodomain LCEs films were synthesised following a procedure published previously[6,12] and described briefly herein. The chemical components of the unpolymerized precursor mixture are shown in Fig. 1c and are as follows: a monofunctional mesogen (A6OCB); a bifunctional mesogenic cross-linker (RM82); a monofunctional non-mesogenic component (EHA); a non-reactive mesogen (6OCB) which is included in the mixture to broaden the nematic phase range of the monomer mixture;[12,31] and a photoinitiator (MBF). The mesogenic cross-linker (RM82), mesogenic side group (A6OCB) and non-reactive mesogen (6OCB) are stirred in the isotropic phase at 120 °C for 5 minutes and then cooled to approximately 50 °C. The non-mesogenic side group (EHA) and the photointiator (MBF) are then added to the mixture and stirred at 50 °C for a further 2 minutes.

The mixture is filled in the nematic phase into a mould to form an aligned, monodomain LCE film. The mould is constructed of a glass microscope slide (7.5 cm × 2.5 cm × 1 mm) and a 250 μm thick Melinex ST725 film (7 cm × 2.5 cm × 250 μm, DuPont Teijin films) separated by 100 μm thick Melinex spacers sandwiched and glued with UVS91 (Norland Products Inc.) to ensure an even spacing between the two substrates. Before construction, the substrates are spin-coated with an aqueous 0.5%/wt polyvinyl alcohol (M_w = 13 000–23 000, Sigma Aldrich) solution, thermally annealed at 50 °C for 15 minutes, and finally rubbed in a preferential direction with a velvet cloth to achieve a monodomain surface alignment. Once the mould is filled, the mixture is left at room temperature for 20 minutes, after which it is UV photopolymerised (2.5 W cm^{-2}) for 2 hours ensuring a full cure. After curing, the LCE is removed from the mould by peeling away the flexible Melinex substrate and subsequently running a scalpel blade between the film and glass substrate. The unpolymerized components (including the 6OCB) are washed out using a 30 : 70 dichloromethane (DCM) and isopropyl alcohol (IPA) solution. DCM is a good solvent of 6OCB, however, pure DCM will result in samples tearing due to swelling too fast.[12] The 30 : 70 DCM : IPA mixture is used to prevent this. The nematic LCE film is dried at room temperature for 5 hours. This step is a requirement as upon polymerisation the LCE is formed in a swollen state washing out 6OCB and subsequent drying of the film results in monodomain network.[12,31]

Strain-mechanical analysis and director tracking

Strain–strain measurements were performed using bespoke equipment comprising of two linear actuators and polarised optics allowing for strain measurements with simultaneous bright-field or polarised microscopy images. An in-depth description of the equipment, along with the methodology to process data, has been published previously.[6,12] In brief, a ~0.1 mm thick sample of dimensions 10 mm × 2 mm is loaded between the two actuators and the initial gauge length is set to remove any slack within the sample. The geometry used

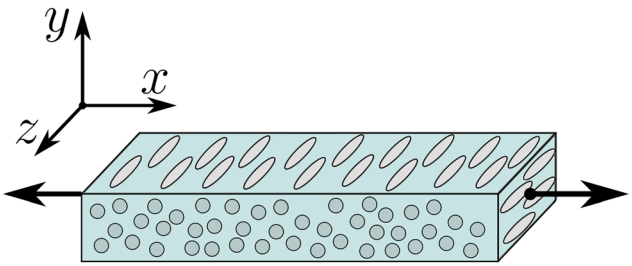

Fig. 2 Geometry and alignment of LCEs in this study. The nematic director in the unstrained LCEs is along the *z*-axis, strain is applied along the *x*-axis. The thickness of the LCE, *i.e.* the dimension in which the auxetic response is observed, is along the *y*-axis.

for strain–strain measurements is shown in Fig. 2. During strain measurements, unpolarised and polarised images of the sample are taken in the *x*–*z* plane. Particle tracking is then used to deduce the *x*-strain and *z*-strain of the sample. The *y*-strain, $\varepsilon_{y,\mathrm{eng}}$, defined in eqn (1) is inferred through the principle of conservation of volume, known to be a valid approach for these auxetic LCEs.[6,8]

$$\varepsilon_{y,\mathrm{eng}} = \frac{1}{(1+\varepsilon_{x,\mathrm{eng}})(1+\varepsilon_{z,\mathrm{eng}})} - 1, \tag{1}$$

where $\varepsilon_{i,\mathrm{eng}}$ is the engineering strain in the *i*-th axis. In all cases, unless specified, the strain is shown in the true strain ($\varepsilon_{\mathrm{true}}$) representation given by eqn (2):

$$\varepsilon_{\mathrm{true}} = \ln(\varepsilon_{\mathrm{eng}} + 1) = \ln\left(\frac{L}{L_0}\right), \tag{2}$$

where L is the sample length and L_0 is the initial sample length. The Poisson's ratios of the samples were determined from the strain–strain measurements using eqn (3):

$$\nu_{xy} = -\frac{\partial\varepsilon_{y,\mathrm{true}}}{\partial\varepsilon_{x,\mathrm{true}}}, \tag{3}$$

where ν_{xy} is the Poisson's ratio in the axis in which the auxetic response is observed.

The director angle was determined from the polarised images of the sample as described previously.[12] The transmitted light intensity for each strain step is recorded under cross-polarised conditions in 10° increments for a full 360° rotation. For each strain step the transmitted intensity as a function of cross-polarised angle is fitted with eqn (4) to determine the director angle of the sample.

$$I = I_0 \sin^2\left(\frac{b\pi \times (\varphi - c)}{180}\right) + d, \tag{4}$$

where I is the average intensity for a 100 × 100 pixel region of interest at the centre of LCE sample, φ is the angle between the polariser and the fast axis of the sample in the *z*–*x* plane, I_0, b, c and d are fitting parameters.

Stress–strain mechanical analysis

Uniaxial stress–strain measurements were performed using a TA Instruments DMA 850 with a film tension clamp. Samples were loaded lengthways between the sample clamps and strained perpendicular to the LC director (geometry shown in Fig. 2) at the chosen strain rate until the desired maximum strain is reached. A strain rate of 0.1% min^{-1} was used as this ensured that measurements were sufficiently slow to be considered "quasi-static" and not influenced by any relaxation dynamics. From the stress–strain measurements, the true stress was calculated using eqn (5):

$$\sigma_{\mathrm{true}} = \left(\frac{L}{L_0}\right)\sigma_{\mathrm{eng}} = \left(\frac{L}{L_0}\right)\frac{F}{A_0}, \tag{5}$$

where F is the force measured by the transducer, and A_0 is the initial cross-sectional area of the sample.

Differential scanning calorimetry (DSC)

DSC measurements were performed to determine the phase behaviour of the samples using a TA Instruments Q2000 with a RCS90 cooling system. 8–12 mg of sample (or ∼10 μL of solution) was hermetically sealed within a TZero aluminium pan. The sample was heated above T_g to 80 °C and held for 5 minutes to maximise thermal contact between the sample and the pan. Heat flow was measured on cooling from 80 °C at −10 °C min^{-1} to −60 °C, holding for 2 minutes, then heating from −60 °C at 10 °C min^{-1} to a maximum temperature selected based on the sample composition (80–180 °C), then holding for 2 minutes. This cycle was repeated 3 times to ensure no thermal degradation, mass loss, or other effects. A rate of 10 °C min^{-1} has been shown to correspond well to a structural relaxation time of ∼100 s in many polymeric and non-polymeric systems including LCEs,[18,32,33] the transition temperature of which is often defined as the glass transition temperature (T_g).[34] In this work, T_g was taken as the inflection point of the step change in heat flow corresponding to the glass transition on cooling. For the relevant LCE samples, the transition temperature from nematic to isotropic (T_{NI}) was taken as the point of change in gradient of the derivative heat flow on heating. This overcame the difficulties in deconvoluting the weak continuous nematic to isotropic transition from the baseline heat flow. For the unpolymerized solutions, $T_{NI,p}$ (with the subscript denoting precursor) was defined as the onset of the peak in heat flow on cooling at a rate of 10 °C min^{-1} during cycling from −60 °C to 80 °C.

Thermal actuation measurements

The shape-change of LCEs can offer insight into a nematic–isotropic phase transition and dimensional variation was determined as a function of temperature using a Linkam LTS350 hot-stage attached to a Linkam TMS93 controller, recording images of the sample dimensions with a Ximea xiQ MQ042CG-CM camera. To reduce the adhesion of the sample to the surface, the LCEs were placed on a glass cover slip which was coated in a thin layer of silicon oil (Sigma Aldrich). A heating rate of 2 °C min^{-1} was used for all samples and the maximum temperature was selected between 100–250 °C based on the material's T_{NI}. In all cases, the starting temperature of the measurement was 25 °C. The recorded images were analysed in

ImageJ where the length of the sample parallel ($L_{\parallel}$) and perpendicular ($L_{\perp}$) to the director was determined from the average of 3 measurements along or across the sample. Due to the coupling between the mesogenic order and the macroscopic shape of the LCE, an effective T_{NI} for the relevant LCEs could be determined by taking the differential of $L_{\parallel}$ with respect to T which can be compared to T_{NI} determined from DSC measurements.

Order parameter measurements

The uniaxial order parameters $\langle P_2\rangle$ and $\langle P_4\rangle$ were determined *via* polarised Raman spectroscopy as described in detail in previous publications for LCEs and liquid crystals systems.[7,8,35,36] The procedure for determining order parameters *via* Raman spectroscopy is briefly described as follows.

The uniaxial order parameters are determined using monodomain nematic LCE samples with the nematic director aligned in the x–z plane. The laser beam propagates in the y direction with the polarisation in the x–z plane. The nematic director is therefore at some angle, θ, with respect to the polarisation of the incoming laser. The intensity of the back-scattered signal of the selected Raman vibrational mode parallel ($I_{\parallel}$) and perpendicular ($I_{\perp}$) to the incident laser polarisation is recorded as a function of θ. For a uniaxial phase comprised of uniaxial molecules, $I_{\parallel}$ and $I_{\perp}$ are related to the uniaxial order parameters ($\langle P_2\rangle$, $\langle P_4\rangle$) through eqn (6) and (7):

$$I_{\parallel} \propto \frac{1}{5}+\frac{4p}{15}+\frac{8p^2}{15}+\langle P_2\rangle \times \left[\frac{1}{21}\left(3+p-4p^2\right)(1+3\cos(2\theta))\right] + \langle P_4\rangle \times \left[\frac{1}{280}(1-p)^2\times(9+20\cos(2\theta)+35\cos 4(\theta))\right] \quad (6)$$

$$I_{\perp}(\theta) \propto \frac{1}{15}(1-p)^2+\langle P_2\rangle \times \left[\frac{1}{21}(1-p)^2\right] + \langle P_4\rangle \times \left[\frac{1}{280}(1-p)^2\times(3-35\cos(4\theta))\right] \quad (7)$$

where p is the differential molecular polarisability. Fitting of eqn (6) and (7) is performed through considering the depolarization ratio, $R(\theta) = I_{\perp}/I_{\parallel}$, which removes the dependence of the fitting on the incident laser intensity. The Raman depolarization data were collected using a Renishaw inVia system (532 nm, 500 mW solid-state laser) which employs a Leica DM2700P polarizing microscope equipped with a rotating stage. Measurements were recorded in $\theta = 10^{\circ}$ increments using a 20× objective with 5% laser power. The 1606 cm^{-1} Raman mode, which is associated with the C–C stretch of the biphenyl rings of the mesogenic units, was selected as it is the bond vibration which most closely agrees with the assumptions underlying the determination of order parameters *via* Raman spectroscopy.[35]

Polarised optical microscopy for strain relaxation images

Polarised optical microscopy was performed using a Leica DM2700P polarised light microscope with a white light LED source, crossed polarisers, a 0.9 numerical aperture condenser lens and a 20× objective. Images of the LCEs were taken on unstrained samples which were then deformed to the desired strain using a bespoke straining rig which can be housed on top of the rotating stage of the microscope. Images were then taken of the strained sample after a desired relaxation time. The scale of the images was calibrated using a microscope graticule.

X-ray scattering

Wide angle X-ray scattering (WAXS) measurements were recorded under vacuum and at room temperature using an Anton Paar SAXSPoint 5.0 equipped with a K-α Cu source (1.5418 Å) and a Dectris EIGER2 R 1M detector (1028 × 1062 pixel array). Measurements were performed by exposing the samples to a 2 mm diameter beam for 5 minutes and repeated for a total of 3 frames which were then averaged. Measurements were performed beam stop-less and a background scan was performed at the same detector position which was subtracted from the measurements. 2D data reduction was performed by azimuthally integrating the 2D X-ray pattern whilst masking the central contribution related to the non-scattered X-ray beam.

Results

LCE material synthesis and physical properties

A series of chemically similar LCEs were produced in which the cross-link density of the system was varied by sequentially halving the mass of RM82 in the precursor mixture whilst keeping the mass of all other components constant. The chemical compositions of both the precursor mixtures and the final LCEs used in this work are shown in Table 1 and are reported in mol% for convenience. The LCE samples in Table 1 are labelled such that the auxetic material from Wang *et al.*[8] is the reference LCE, labelled "1×", while the 2× material has comparable cross-link density to the material reported by Mistry *et al.*[12] albeit with slightly different ratios of A6OCB and EHA. The labels indicate the approximate amount of RM82 cross-linker in the precursor solution relative to that in Wang *et al.*, *e.g.* 1/2× contains half the amount of cross-linker as 1×. It can be seen that the final LCEs vary in their cross-linker concentration, the ratio A6OCB : EHA remains consistent, and the total mesogenic content varies from 66.3 mol% (2× LCE) to 60.6 mol% (1/16× LCE).

Table 1 The chemical compositions of the precursor mixture and the final polymerised LCEs (after 6OCB and MBF were washed out)

	Precursor mixture (mol%)					Final LCE (mol%)		
Sample	A6OCB	EHA	RM82	6OCB	MBF	A6OCB	EHA	RM82
2×	23.6	15.4	6.8	52.8	1.4	51.5	33.7	14.8
1×	24.4	16.0	3.5	54.6	1.5	55.6	36.4	8.0
1/2×	24.8	16.2	1.8	55.6	1.5	58.0	37.9	4.2
1/4×	25.1	16.4	0.9	56.1	1.5	59.2	38.7	2.1
1/8×	25.2	16.5	0.5	56.4	1.5	59.8	39.1	1.1
1/16×	25.2	16.5	0.2	56.5	1.5	60.1	39.3	0.5

Table 2 The transition temperatures of samples investigated *via* DSC and thermo-actuation measurements. Note that T_{NI} was not observed for the 2× sample using either method and a value could not be discerned for the 1× sample using DSC

	DSC precursor	DSC LCE		Thermo-actuation LCE
Sample	$T_{NI,p}$ (°C)	T_{NI} (°C)	T_g (°C)	T_{NI} (°C)
2×	46.5 ± 0.2	—	18 ± 1	—
1×	41.2 ± 0.2	—	13 ± 1	120 ± 10
1/2×	37.2 ± 0.2	63 ± 2	8 ± 1	72 ± 5
1/4×	35.6 ± 0.2	48 ± 2	6 ± 1	55 ± 2
1/8×	33.7 ± 0.2	38 ± 2	2 ± 1	40 ± 2
1/16×	32.7 ± 0.4	32 ± 2	0 ± 1	34 ± 2

The transition temperature temperatures of the LCE precursors and films were characterized by differential scanning calorimetry (DSC), the results of which are shown in Table 2. A cooling rate of 10 °C min^{-1} was used and the inflection point of the glass transition step was chosen to define T_g (Fig. 3a). The glass transition temperatures reduce with a reducing cross-link density, with an approximately 20 °C difference between the highest and lowest cross-linked systems. A contributing factor to this will be the corresponding increase in the mol% of the flexible side-groups, A6OCB and EHA in the films; the latter acts as a plasticiser and increases from 33.7 mol% to 39.3 mol% across the series. The nematic-to-isotropic transition behaviour of both the LCE films (Fig. 3a) and the precursor mixtures (Fig. S1) was also determined. The nematic to isotropic transition for the precursor mixtures all have a clear transition enthalpy and can be defined as weakly 1st order; they are easy to determine *via* DSC. In all cases, $T_{NI,p}$ of the precursor mixtures are well-above room temperature, ensuring that the materials are polymerised in the nematic phase. However, T_{NI} is much more difficult to distinguish for the LCE films (Fig. 3a), as is expected for the softened transition observed in LCEs[22] and becomes more visible in the differential of the DSC trace, dQ/dT (Fig. 3b). Thus T_{NI} for the LCEs is taken as the point of change in gradient of the derivative heat flow on heating.

An alternative approach to determining T_{NI} of the LCE films involves monitoring the thermal actuation (contraction) in the direction parallel to the director upon heating (Fig. 3c and d). In Fig. 3c, the data are normalised to 1 at the highest temperatures and Fig. 3d shows the rate of change of length with respect to temperature ($\partial L_\parallel/\partial T$, normalised such that the minimum is −1). T_{NI} determined from the thermo-actuation measurements has been defined as the minimum in $\partial L_\parallel/\partial T$ (Fig. 3d, shown by vertical dashed lines). Reasonable agreement between the values from both techniques is found with agreement within experimental error. Both techniques show that T_{NI} increases with cross-link density. It is worth noting that the thermal actuation data, unlike the DSC data, suggest a transition for the 1× LCE, which is undetectable for the "2×" material and other auxetic LCEs with comparable cross-link densities.[12,18] Further evidence for a nematic-to-isotropic transition at ∼120 °C in the 1× LCE is provided in the SI *via* transmission spectroscopy (Fig. S2) and fluorescence spectroscopy (Fig. S3). As can be seen from Fig. 3b and d, as the cross-link density of the LCE increases, the T_{NI} of the LCEs increases and the transition broadens, becoming more continuous. The broadening of the nematic-to-isotropic transition in LCEs has previously been shown to depend on cross-link density[22,37,38] and has been related to an underlying internal mechanical field in nematic LCEs which effectively alters the Landau De Gennes energy leading to a super-critical behaviour.[22,39] We explore this point in the next section of the manuscript.

The room-temperature order parameters of the LCEs determined *via* polarised Raman spectroscopy are shown in Fig. 3e. Upon increasing mesogenic content, both uniaxial order parameters increase, $\langle P_2\rangle$ taking a maximum value of 0.64 ± 0.05 for the 2× sample (14.8 mol% RM82) while a minimum value of 0.37 ± 0.05 is observed for the 1/16× sample (0.5 mol%). This behaviour is as expected for systems polymerised at temperatures that differ from $T_{NI,p}$ in the precursor mixture by different amounts; the order parameter of the precursor mixture is to some extent locked in during curing.[14] In this case, $T_{NI,p}$ reduces monotonically from the highest (2×) to lowest (1/16×) cross-link density precursor material. Plotting $\langle P_4\rangle$ against $\langle P_2\rangle$ allows one to determine any trends within the order parameter independent of an external variable,[19] commonly temperature, however, in this case cross-link density. The $\langle P_2\rangle$ *vs.* $\langle P_4\rangle$ phase space representation of Fig. 3(e) is shown in Fig. S4. In Fig. 3e, the grey line represents $\langle P_4\rangle$ for the measured $\langle P_2\rangle$ as predicted by the mean-field Maier–Saupe theory showing excellent agreement with the measured values of $\langle P_4\rangle$. Thus, changing the cross-link density significantly effects the room temperature order parameters of the LCEs, but the form of the orientational distribution function in each of the LCEs is effectively the same (follows Maier–Saupe predictions and is thus a singly peaked Gaussian distribution centred at $\beta = 0°$). This is likely due to the LCE being cross-linked within the conventional LC nematic phase.

LCE order parameter *vs.* temperature and internal field

Motivated by the findings in the previous section, that increased cross-link density both increases and broadens the T_{NI} of the LCE series, a modified Maier–Saupe model is presented that describes the unstrained LCE as a function of temperature. We emphasise that the theory is not aimed at describing an LCE under external strain, rather, our approach aims to both aid in understanding the role of internal strain and to attempt to quantify it in these LCEs by describing the influence of internal strain on the temperature-dependent order parameter. Based on previous publications[40,41] and the Maier–Saupe theory of nematic liquid crystals,[42,43] we suggest a free energy, F, of the liquid crystal elastomer of the following phenomenological form, eqn (8) (further details of assumptions and previous work are given in the SI). Specifically, we are proposing a description of the order parameter temperature dependence in an LCE by using the free energy which is a sum of the mesogenic groups free energy within the frame of the Maier–Saupe free energy (F_{MS}), coupling of the orientational ordering and strain

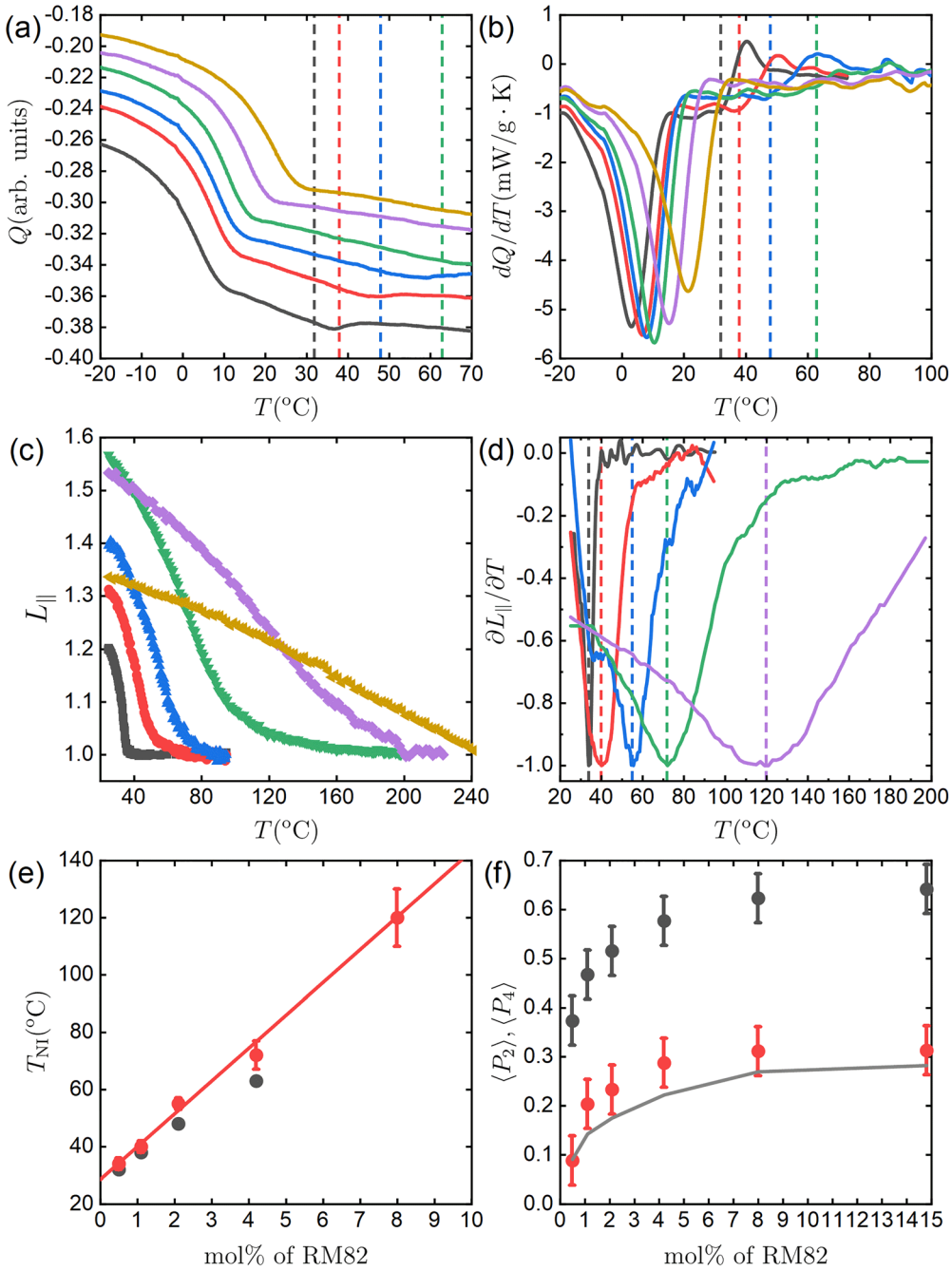

Fig. 3 Physical properties of the LCEs where black = 1/16×, red = 1/8×, blue = 1/4×, green = 1/2×, purple = 1×, and yellow = 2× RM82 sample. (a) Heat flow, Q, of the LCE series (offset, top 2× RM82 sample, bottom 1/16× RM82 sample) as determined *via* DSC, displaying clear glass transitions. (b) Temperature differential of heat flow (dQ/dT) determined by DSC for the LCE series. In addition to clear peaks at lower temperatures associated with T_g, coloured vertical lines show the point taken as T_{NI} (c) thermal contraction (actuation) of the LCE parallel to the nematic director ($L_\parallel$) determined on heating. (d) Temperature differential of the thermal contraction of the LCE parallel to the nematic director upon heating ($\partial L_\parallel/\partial T$). The vertical-coloured lines show the points taken as T_{NI}. (e) T_{NI} measured *via* DSC (black, onset of peak in dQ/dT for the elastomers) and thermo-actuation measurements (red, peak of $\partial L_\parallel/\partial T$). (f) Uniaxial order parameters, ($\langle P_2\rangle$ (black) and $\langle P_4\rangle$ (red)), of the LCE series at room temperature determined *via* Raman spectroscopy. The grey solid line is the value of $\langle P_4\rangle$ predicted from $\langle P_2\rangle$ using Maier–Saupe theory.

($U\varepsilon_I S$), and rubber elasticity $\left(-\sigma\varepsilon_I + \frac{1}{2}\mu\varepsilon_I^2\right)$. The phenomenological form of the F energy is given in eqn (8):

$$F = F_{MS} - U\varepsilon_I S - \sigma\varepsilon_I + \frac{1}{2}\mu\varepsilon_I^2. \quad (8)$$

The first term is the classical Maier–Saupe free energy of mesogenic groups:

$$F_{MS} = \frac{\alpha S^2}{2} + k_B T \times \ln(Z), \quad (9)$$

$$Z = \frac{1}{\int_0^{\pi} \exp\left(-\frac{\nu(S,\theta)}{k_B T}\right) \sin(\theta) d\theta}, \quad (10)$$

$$\nu(S,\theta) = -\alpha S P_2(\cos(\theta)). \quad (11)$$

In eqn (8)–(11), $S = \langle P_2 \rangle = \langle P_2(\cos(\theta)) \rangle$ is the order parameter, $P_2(\cos\theta)$ is the second Legendre polynomial, k_B is the Boltzmann constant and α is a constant related to interparticle spacing. The second term in (8) $-U\varepsilon_I S$ describes the coupling between the orientational order parameter and the internal strain ε_I. The third term $-\sigma\varepsilon_I$ is the contribution due to the stress σ, acting on the elastomer, which is a combination of the applied stress and the internal stress due to anisotropic cross-linking (note that in these experiments the films are under no applied stress so σ is purely the internal stress), and $\frac{1}{2}\mu\varepsilon_I^2$ describes the elastic part of the LCE free energy where μ is the Lamé parameter.[41]

To find the order parameter and strain, one needs to minimize the total free energy, eqn (8), with respect to S and ε_I. The necessary condition for an extremum is:

$$\frac{\partial F}{\partial S} = \alpha S + k_B T \frac{\partial Z/\partial S}{Z} - U\varepsilon_I = 0, \quad (12)$$

$$\frac{\partial F}{\partial \varepsilon_I} = -US - \sigma + \mu\varepsilon_I = 0. \quad (13)$$

From eqn (13) we find:

$$\varepsilon_I = \frac{US + \sigma}{\mu}. \quad (14)$$

By substituting eqn (14) into eqn (12) we get:

$$\frac{\partial F}{\partial S} = \alpha S + \frac{\alpha}{2} + \frac{3\alpha}{2} \frac{\int_0^1 x^2 \exp\left(\frac{3\alpha}{2k_B T} S x^2\right) dx}{\int_0^1 \exp\left(\frac{3a}{2k_B T} S x^2\right) dx} - \frac{U^2 S + \sigma U}{\mu}. \quad (15)$$

It is convenient to measure all energy parameters (a, μ, σ, U) in reduced $k_B T$ units noting that in the classical Maier–Saupe theory the ratio $\frac{a}{k_B T_C} \approx 4.55$.[43] Note that here we have used T_C as opposed to T_{NI} as T_C isn't necessarily the temperature associated with the observed nematic to isotropic phase transition but rather what would be seen in the absence of an internal field and is a fitting parameter like U, σ and μ. Thus to find $S(T/T_C)$ one needs to numerically solve the eqn (16):

$$\tilde{a}S + \frac{\tilde{a}}{2} - \frac{3\tilde{a}}{2} \frac{\int_0^1 x^2 \exp\left(S\frac{3\tilde{a}}{2}\frac{T_C}{T}x^2\right) dx}{\int_0^1 \exp\left(S\frac{3\tilde{a}}{2}\frac{T_C}{T}x^2\right) dx} - \frac{\tilde{U}^2 S + \tilde{\sigma}\tilde{U}}{\tilde{\mu}} = 0, \quad (16)$$

where $\tilde{a} = a/k_B T_C = 4.55$, and the other non-dimensional parameters $\tilde{U} = U/k_B T_C$, $\tilde{\sigma} = \sigma/k_B T_C$, $\tilde{\mu} = \mu/k_B T_C$ are unknown fitting parameters.

Fig. 4 shows fittings to the order parameter data obtained *via* Raman spectroscopy as a function of temperature ($S = \langle P_2 \rangle$)

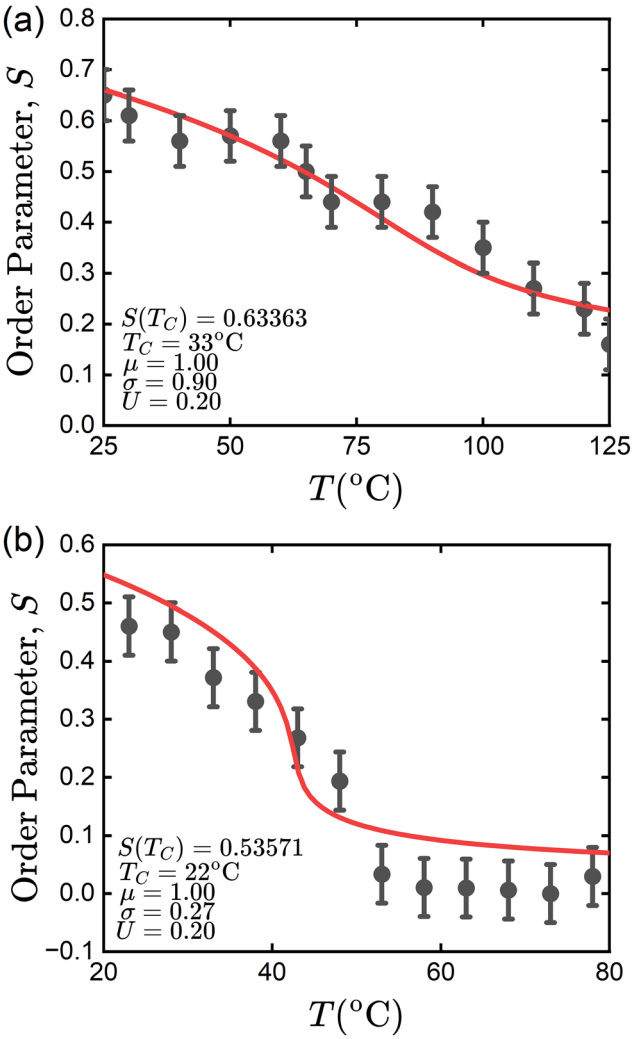

Fig. 4 Order parameter ($S = \langle P_2 \rangle$) data obtained from Raman spectroscopy measurements for (a) 1× sample and (b) 1/8× sample. The red lines show the numerical fit to the data by solving eqn (16), with the relevant fitting parameters shown for each case.

for two of the LCE films. The fits are obtained by numerically solving eqn (16) for the 1× sample (Fig. 4a) and the 1/8× sample (Fig. 4b). Two of the parameters are identical for both fits; U = 0.2, μ = 1 and it can be seen that the fits offer a reasonable representation of the data. Importantly, the results of Fig. 4 show that an increased cross-link density is associated with larger internal stresses with the 1× LCE's internal stress parameter (σ = 0.9) being ~3.3 times greater than that of the 1/8× LCE (σ = 0.27). Additionally, we can see from Fig. 4 that increased cross-link density is associated with a higher value of T_C. The parameter T_C is connected with the orientational interaction between mesogenic groups, thus a higher T_C means a stronger orientational interaction.

Mechanical behaviour

The stress–strain responses of the LCEs were measured as described in the experimental section at a strain rate of 0.1% min^{-1}, perpendicular to the director, Fig. 5a and b, the altered

scale Fig. 5b allowing the details of a the "S"-shaped response associated with the SSE response to be seen for the 1/2× and lower cross-linked samples. The data can be considered in the context of which show "S"-like stress–strain responses, *i.e.* a low modulus plateau after an initial critical strain which is a hallmark of SSE behaviour. The 2×, 1× and 1/16× samples do not show such behaviour, though the 1/8×, 1/4× and 1/2× samples clearly do. The lack of a robust "S"-shaped characteristic in the stress–strain response of the 1/16× sample is likely due to the low order parameter (0.37 ± 0.05) in the system and proximity of measurement (23 °C) to T_{NI} (32 °C) suggesting that there is not a robust enough nematic order or coupling in the system to elicit the semi-soft response for a monodomain sample in this LCE.[44–46]

The initial elastic modulus, E_0, for each of the LCEs is determined by taking the gradient of the stress–strain curves near $\varepsilon_{x,true} = 0$ and values of E_0 are presented in Table 3. It can be seen that E_0 increases monotonically with the cross-link density, as predicted for a cross-linked network.[47] However, the role of T_g on E_0 must also be noted, especially as the measurement temperature (23 °C) is rather close to T_g for the films with higher cross-linking, meaning that a strain rate of 0.1% min^{-1} may not be sufficiently slow to ensure a quasi-static measurement and hence the dynamic response of the LCE can become

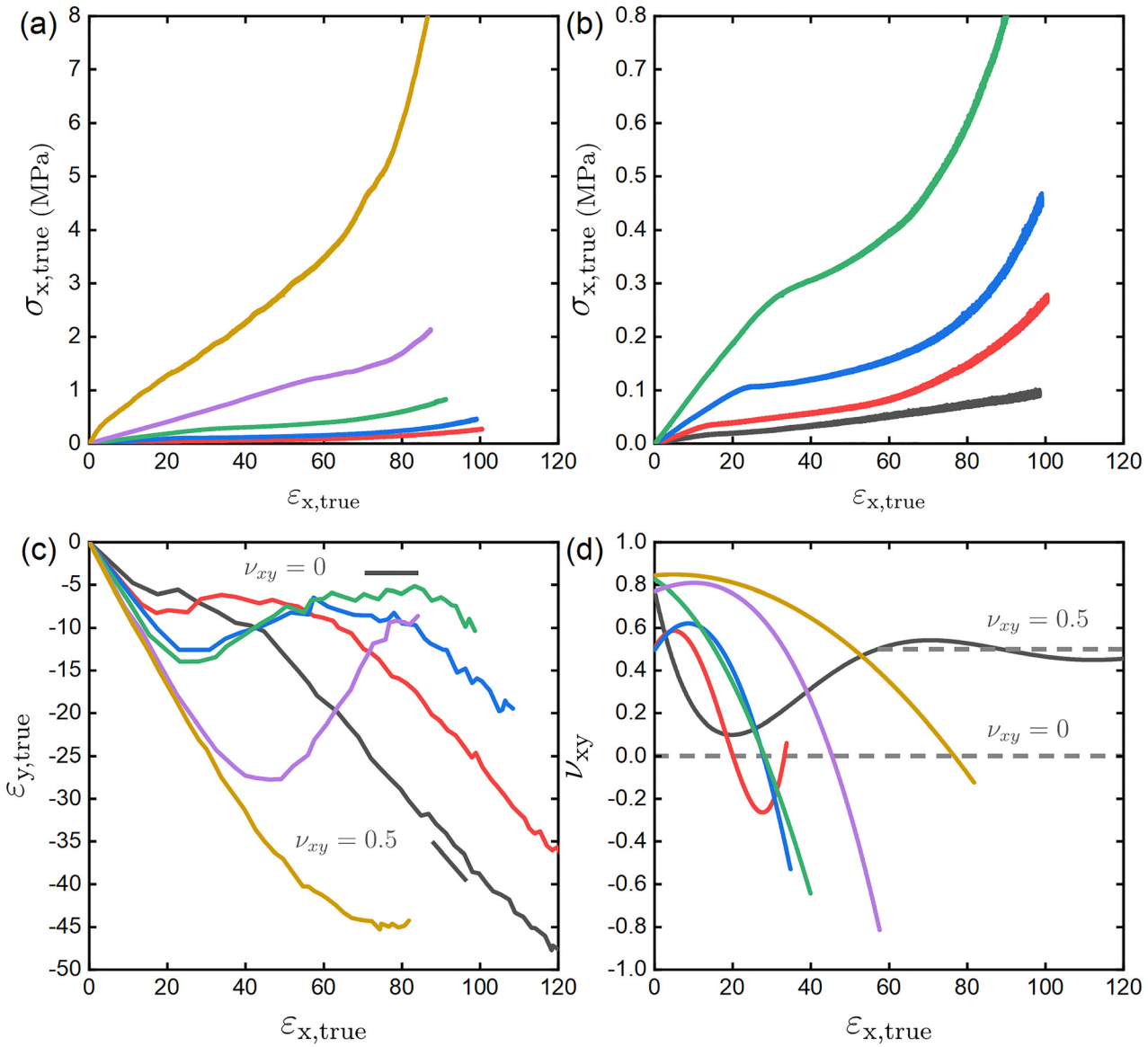

Fig. 5 Mechanical deformation behaviour of the LCEs where black = 1/16×, red = 1/8×, blue = 1/4×, green = 1/2×, purple = 1× and yellow = 2× RM82 sample. (a) True stress (σ_x) *vs.* true strain (ε_x) in the *x*-direction at a strain rate of 0.1% min^{-1}; (b) true stress (σ_x) *vs.* true strain (ε_x) in the *x*-direction focusing on the lower cross-link density samples at a strain rate of 0.1% min^{-1}; (c) true strain (ε_y) in the *y* direction *vs.* true strain (ε_x) in the *x* direction at a strain rate of 0.5% min^{-1} and (d) instantaneous *x*–*y* Poisson's ratio (ν_{xy}) *vs.* true strain (ε_x) in the *y* direction at a strain rate of 0.5% min^{-1}. Note that ν_{xy} of the 1/16× samples was calculated over the full strain range to demonstrate the collapse of the behaviour onto the ν_{xy} = 0.5 line.

Table 3 The mechanical properties of the family of LCEs, including the Young's modulus (E_0), the threshold strain at which the system becomes auxetic ($\varepsilon_{(\nu<0)}$). All values were determined at 23 °C

Sample	E_0 (MPa)	$\varepsilon_{(\nu<0)}$ (%)
2×	11.7 ± 0.8	77 ± 5
1×	2.3 ± 0.4	45 ± 5
1/2×	0.97 ± 0.05	28 ± 5
1/4×	0.49 ± 0.06	28 ± 5
1/8×	0.26 ± 0.04	20 ± 5
1/16×	0.20 ± 0.04	—

important. Fig. S5 shows the dependence of E_0 on both the cross-link density and T_g.

The auxetic response is investigated using the bespoke apparatus and a strain rate of 0.5% min^{-1} was selected to match previous work on auxetic LCEs.[8,9,17] Fig. 5c shows the *y*-strain *vs.* *x*-strain data (geometry consistent with Fig. 2) from which the instantaneous Poisson's ratio was calculated, Fig. 5d, using eqn (3). Table 3 shows both the critical strains (auxetic thresholds) $\varepsilon_{(\nu<0)}$ and E_0 which increases with increasing cross-link density up to the 1× sample (8.0 mol% RM82). All the LCEs apart from the lowest cross-linked sample show some auxetic behaviour though the 2× sample fails just beyond its auxetic threshold $\varepsilon_{(\nu<0)}$ so a significant auxetic response was not observed. The 1/16× sample displays no evidence of auxeticity and instead follows behaviour close to ν_{xy} = 0.5, expected for an isotropic rubber, throughout the deformation.[48] This is further evidence, along with lack of a characteristic "S"-shape stress–strain curve that the nematic order in this LCE is not robust and the coupling is weak. It is especially interesting that the moderately-crosslinked LCEs (1/2×, 1/4× and 1/8×) all show at least a small auxetic response, despite also showing clear SSE-like behaviour. The data of Fig. 5 and Table 3 show that the auxetic threshold reduces as the cross-link density reduces (see also Fig. S5). A dependence of the auxetic threshold on T_g was found for a series of acrylate LCEs with identical cross-link densities, differing only in the spacer length of the attaching the mesogenic side-chain; samples with higher T_g display larger threshold strains.[17] This behaviour is also seen for the LCEs described here, Fig. S5, where the auxetic strain threshold increases rapidly as T_g approaches room temperature (where the experiments were carried out).

The details of the strain–strain data also reveal some interesting behaviour. The intermediate cross-link density LCEs (1/8×, 1/4× and 1/2×) display an auxetic response at relatively small strains followed by a recovery and a strain region where the *y*-strain does not change with *x*-strain (shown by ν_{xy} = 0 line in Fig. 5c which is quite apparent for the 1/2× LCE). Following this, the strain–strain response tends towards that of an isotropic rubber or of a uniaxial LCE strained along the director (ν_{xz} = 0.5).[2] Interestingly, the strain–strain behaviour at and above the ν_{xy} = 0 plateau is indicative of the semi-soft elasticity where a flat strain–strain response in the *y*-dimension occurs in the region in which there is uniaxial, in-plane rotation of the nematic director in the *z*-direction.[2,48] After rotation has completed, the director is aligned with the strain axis and the strain–strain response is that of a classical elastomer.[2,48] The strain–strain behaviour observed in the 1/8×, 1/4× and 1/2× LCEs is therefore clearly auxetic in the low-strain regime, but is reminiscent of the SSE response at higher strains. The existence of an SSE-like response is consistent with the "S"-like stress–strain responses shown in Fig. 5a and b and is explored directly in the following section. However, unlike the classical SSE response which predicts a similar ν_{xy} = ν_{yz} = 0.5 behaviour at small strains before director reorientation occurs,[2,48] the LCES presented herein show clear auxeticity in this strain region. This will be discussed again later in the manuscript. The key point here is to highlight that lower cross-linked LCEs show behaviour with aspects of both the SSE response and the auxetic response with the 1× and 2× LCEs showing behaviour consistent only with a pure auxetic deformation.

Confirmation of the nature of the mechanical behaviour *via* polarising microscopy and X-ray

As discussed in the previous section, all but the lowest cross-link density LCE shows evidence of auxeticity when strained. However, there is also evidence of SSE behaviour through the characteristically low elastic plateau observed in the stress–strain curves and regions of ν_{xy} = 0 and ν_{xy} = ν_{xz} = 0.5 in the strain–strain response for the 1/8×–1/2× samples. As outlined in the introduction, LCEs with pure auxetic behaviour deform biaxially[7,8] and exhibit a hyper-elastic "S"-shaped curve (see 1× in Fig. 5a) which means that such curves cannot be unambiguously associated with either an SSE or a biaxial deformation.[12] Previous investigations of the biaxial auxetic deformation have confirmed that when only the in-plane nematic director is considered (such as occurs in polarising microscopy of planar films), the director appears to rotate sharply after a critical strain is reached.[7,8,12] This is in contrast to the SSE response wherein the director rotates smoothly and continuously in-plane. To gain further insight into the nature of the deformation behaviour of the LCEs studied in this work, we have chosen the 1/8× LCE and the 1× LCE to investigate the behaviour of the director as a function of strain *via* polarised optical microscopy and wide-angle X-ray scattering (WAXS). The 1/8× and 1× LCE are selected since the former most closely follows classical SSE behaviour (only a small auxetic region is suggested in Fig. 4c and the material shows clear plateau and strain hardening behaviour) and the latter has been extensively studied and displays a pure auxetic response.[8]

Fig. 6a shows the angle of the director in the plane of the 1/8× LCE film as a function of applied strain, determined by observation of the samples through rotating crossed polarizers. The director behaviour of the 1/8× LCE is consistent with classical SSE behaviour with continuous rotation of the director after a threshold strain of $\varepsilon_{x,\mathrm{true}} \approx 15\%$ is reached. The start of the director rotation is in the vicinity of the onset of the plateau region of the stress–strain response, as would be expected from the low-energy rotation of the nematic director in the SSE response. In addition to a continuous rotation of the director, the SSE elastic response is typically characterised by the formation of stripe domains which are counter rotating domains

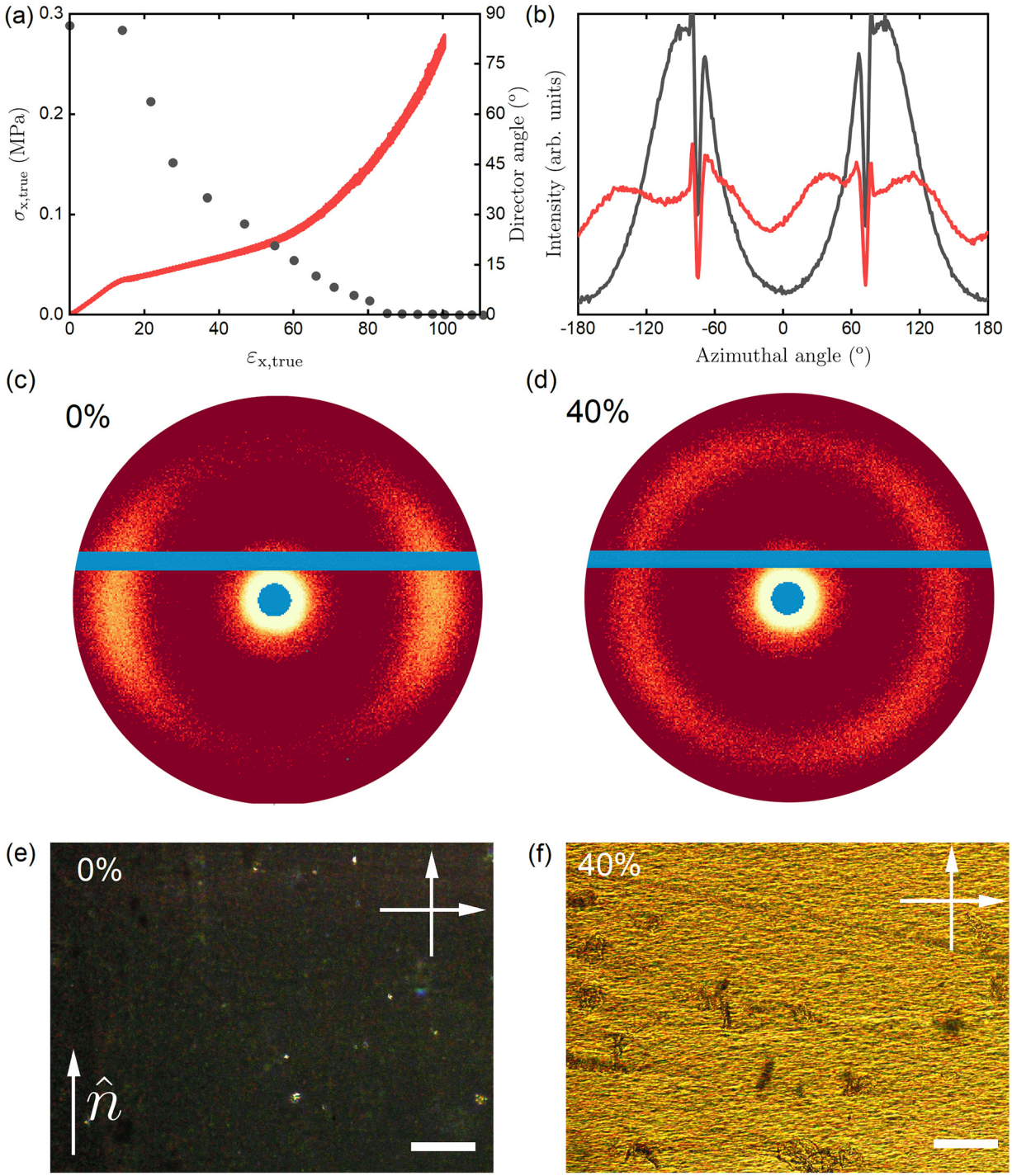

Fig. 6 (a) Stress–strain response of the 1/8× LCE at a strain rate of 0.1% min^{-1} plotted as a function of true-stress ($\sigma_{x,true}$) and true-strain ($\varepsilon_{x,true}$)(red line) and director angle as a function of strain as determined *via* simultaneous observations with crossed polarizers (black circles). (b) X-ray scattering profile as a function of azimuthal angle for the 1/8× sample under $\varepsilon_{x,true}$ = 0% (black) and $\varepsilon_{x,true}$ = 40% (strain). (c) and (d) 2D X-ray scattering image of the 1/8× sample at $\varepsilon_{x,true}$ = 0% and $\varepsilon_{x,true}$ = 40%, respectively. (e) and (f) Polarised optical microscopy images of the 1/8× sample at $\varepsilon_{x,true}$ = 0% and $\varepsilon_{x,true}$ = 40%, respectively. The arrows in (e) and (f) show the direction of the polariser and analyser, $\hat{n}$ defines the orientation of the director in the unstrained sample. Scale bar = 75 μm.

of the director leading to striping along the width of the sample.[1,4,5] The existence of these was investigated *via* WAXS and POM. The 1/8× LCE was measured in the unstrained state and at $\varepsilon_{x,true}$ = 40% strain (*i.e.* within the soft plateau). The black line in Fig. 6b is the azimuthal integration of WAXS pattern of the unstrained 1/8× LCE whereas the red line is the 1/8× LCE at $\varepsilon_{x,true}$ = 40%. The 2D X-ray diffraction images and azimuthal integration of the data of the 1/8× LCE are shown in

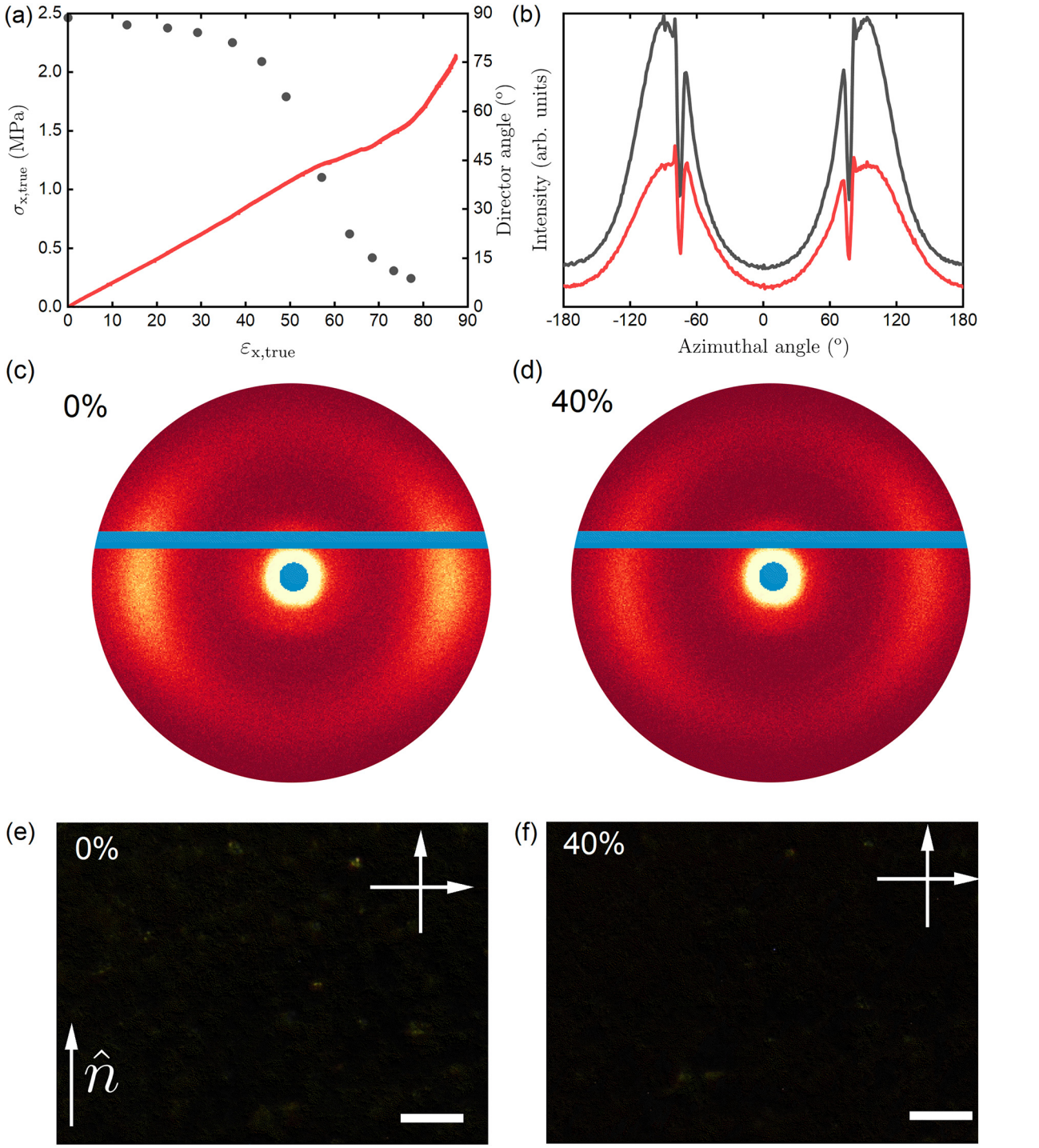

Fig. 7 (a) Stress–strain response of the 1× LCE at a strain rate of 0.1% min^{-1} plotted as a function of true-stress ($\sigma_{x,true}$) and true-strain ($\varepsilon_{x,true}$)(red line) and in-plane projection of the director angle as a function of strain as determined *via* simultaneous observations with crossed polarizers (black circles). (b) X-ray scattering profile as a function of azimuthal angle for the 1× sample under $\varepsilon_{x,true}$ = 0% (black) and $\varepsilon_{x,true}$ = 40% (strain). (c) and (d) 2D X-ray scattering image of the 1× sample at $\varepsilon_{x,true}$ = 0% and $\varepsilon_{x,true}$ = 40%, respectively. (e) and (f) Polarised optical microscopy images of the 1× sample at $\varepsilon_{x,true}$ = 0% and $\varepsilon_{x,true}$ = 40%, respectively. The arrows in (e) and (f) show the direction of the polariser and analyser, $\hat{n}$ defines the orientation of the director in the unstrained sample. Scale bar = 75 μm.

Fig. 6c and d. In the unstrained state the sample shows monodomain nematic ordering with the presence of 2 lobes in the WAXS signal reflecting the side-to-side ordering of the mesogenic units perpendicular to the (vertical) director. Upon straining to $\varepsilon_{x,true}$ = 40%, the WAXS pattern changes, now exhibiting four lobes, suggesting two nematic domains with

their directors at some angle to the original. In this case, for 40% strain, the domains are tilted with their director at $32 \pm 2^{\circ}$ to the original, in excellent agreement with the director rotation depicted in Fig. 6a. The scattering intensity of each of the four lobes is similar, indicating an equal proportion of domains in each direction, as would be expected. The POM (Fig. 6c) shows the uniform LCE prior to strain and then after straining by $\varepsilon_{x,\text{true}} = 40\%$ (the photograph is taken after 10 minutes at this strain). Optical textures consistent with stripe domains can readily be seen indicated by alternating colour regions approximately 5 μm wide. Fig. S6 shows a magnified image of the stripe domain texture and an anisotropic light scattering pattern observed when a 633 nm laser is transmitted through the 1/8× LCE held at $\varepsilon_{x,\text{true}} = 40\%$. The WAXS and POM data, in addition to the anisotropic light scattering pattern,[49] confirm the formation of stripe domains. This information, coupled with the soft elastic plateau (Fig. 3b) confirm that the 1/8× LCE is deforming *via* SSE above the initial small auxetic response.

We now consider the 1× LCE, which displays an auxetic response and has been confirmed by Raman spectroscopy and conoscopy to deform biaxially.[7,8] The 1× LCE behaves quite differently from the 1/8× sample, Fig. 7. In Fig. 7a, it can be seen that the behaviour of the in-plane projection of the director is consistent with the so-called mechanical Fréedericksz transition which is the *x*–*z* plane projection of the director in the auxetic biaxial deformation; there is little to no reorientation until a threshold strain is reached ($\varepsilon_{x,\text{true}} = 43\%$) after which the in-plane projection of the director rotates sharply. In the unstrained state, the sample shows monodomain nematic ordering with the presence of 2 lobes in the WAXS signal (Fig. 7c) reflecting the side-to-side ordering of the mesogenic units perpendicular to the (vertical) director. Upon straining to $\varepsilon_{x,\text{true}} = 40\%$, the WAXS pattern shows a similar pattern to the unstrained state, *i.e.* 2 lobes albeit with a lower scattering intensity (Fig. 7d) which are only slightly shifted in orientation by an angle of $5 \pm 2^{\circ}$ in reasonable agreement with the optical data (Fig. 7a). The reduction in intensity seen in the WAXS data signifies a deformation in which the uniaxial order parameter reduces upon applied strain, consistent with findings *via* Raman spectroscopy and conoscopy in which there is a reduction of uniaxial order parameter, an emergence of biaxial order, and a lack of in-plane director rotation until a threshold strain.[7,8] The differences between the biaxial deformation and SSE are readily demonstrated in the polarized optical microscopy images where the LCE film retains excellent monodomain alignment at $\varepsilon_{x,\text{true}} = 40\%$ (Fig. 7e and f). Such behaviour is consistent with other reports of the optical properties of auxetic LCEs under deformation; no stripe domains are observed and the material remains optically clear throughout, albeit with changed birefringence colours.[6,12]

LCEs are polymer systems so it is to be expected that there is a dependence of the behaviour on the dynamics. The effect of relaxation was investigated on the 1× and 2× LCEs, with the samples held at a strain of $\varepsilon_{x,\text{true}} = 40\%$ for 24 h, Fig. 8a and b. Interestingly, after allowing relaxation for 24 hours the 1× LCE shows a texture consistent with stripe domain formation (Fig. 8b), confirmed by the 2D WAXS data, Fig. 8c and d. This suggests that, despite the fact that the deformation mode of the 1× sample is clearly biaxial (auxetic), at sufficiently long timescales, there is evidence of SSE-like behaviour. The 2× RM82 sample remained optically clear after 24 h (POM images shown in Fig. 8e and f), and even when held at strain for 2 weeks, did not display stripe domain textures, suggesting that at high enough cross-link density, such a relaxation cannot occur.

Dynamic behaviour of the auxetic response in LCEs

Motivated by the results of mechanical testing, POM and X-ray scattering, namely that (i) auxeticity is observed in the low strain region of an LCE deforming *via* SSE and (ii) SSE-like behaviour is observed in an auxetic LCE when sufficient relaxation time is allowed, the effects of dynamics on the strain–strain behaviour was investigated on the 1/8× and 1× LCE sample.

Fig. 9 shows the effects of strain rate on the strain–strain behaviour and the Poisson's ratio of the 1/8× and 1× LCE at a constant temperature of $T = 23\ ^{\circ}\text{C}$. Fig. 9a shows the 1/8× LCE strained at 0.5% min^{-1} (black), 5% min^{-1} (red) and 50% min^{-1} (blue) and Fig. 9b shows the instantaneous Poisson's ratio for the corresponding strain rates. Fig. 9c shows the strain–strain behaviour of the 1× LCE at a strain rate of 0.04% min^{-1} (black), 0.08% min^{-1} (red), 0.5% min^{-1} (blue) and 1% min^{-1} (green), with Fig. 9d again showing the instantaneous Poisson's ratio in each case. In all cases, a higher strain rate increases the auxetic threshold and tends to reduce the magnitude of the auxetic response, which led us to select the strain rates shown for each of the LCEs; the auxetic response in the 1/8× LCE is already small so the strain rate was not reduced below 0.5%. Indeed the magnitude of the auxetic response is comparable for strain rates of 0.5% min^{-1} and 5% min^{-1} in the 1/8× LCE (slightly larger for the latter), while at 50% min^{-1} the system is very barely auxetic (the maximum Poisson's ratio is −0.02). The 1× LCE sample shows a similar behaviour, whereby higher strain rates lead to an increase in the auxetic threshold. However, in this case, strain rates lower than 0.5% min^{-1} were explored as in all cases a robust auxetic response is observed.

A similar effect can be observed by investigating the effect of temperature on the auxetic response at the same strain rate shown in Fig. 10 for the 1× sample. In Fig. 10a, the black line is the strain–strain response of the 1× LCE at a strain rate of 0.5% min^{-1} and $T = 23\ ^{\circ}\text{C}$, the red line is $T = 30\ ^{\circ}\text{C}$ and the blue line is $T = 35\ ^{\circ}\text{C}$. Fig. 9b shows the corresponding instantaneous Poisson's ratio. As the temperature is increased, the auxetic threshold strain reduces, though no particular trend is seen in relation to the magnitude of the response. In polymeric materials, an increase in the strain rate has an equivalence to a reduction in the measurement temperature and in the case of thermorheological simplicity, the two can be super-positioned to form master curves of mechanical behaviour over a wide spans of frequency by performing smaller frequency sweeps at different temperatures.[50] Thus it is expected that a reduction in the auxetic threshold can be achieved by either lower the strain rates (Fig. 9) or investigating at higher temperatures (Fig. 10).

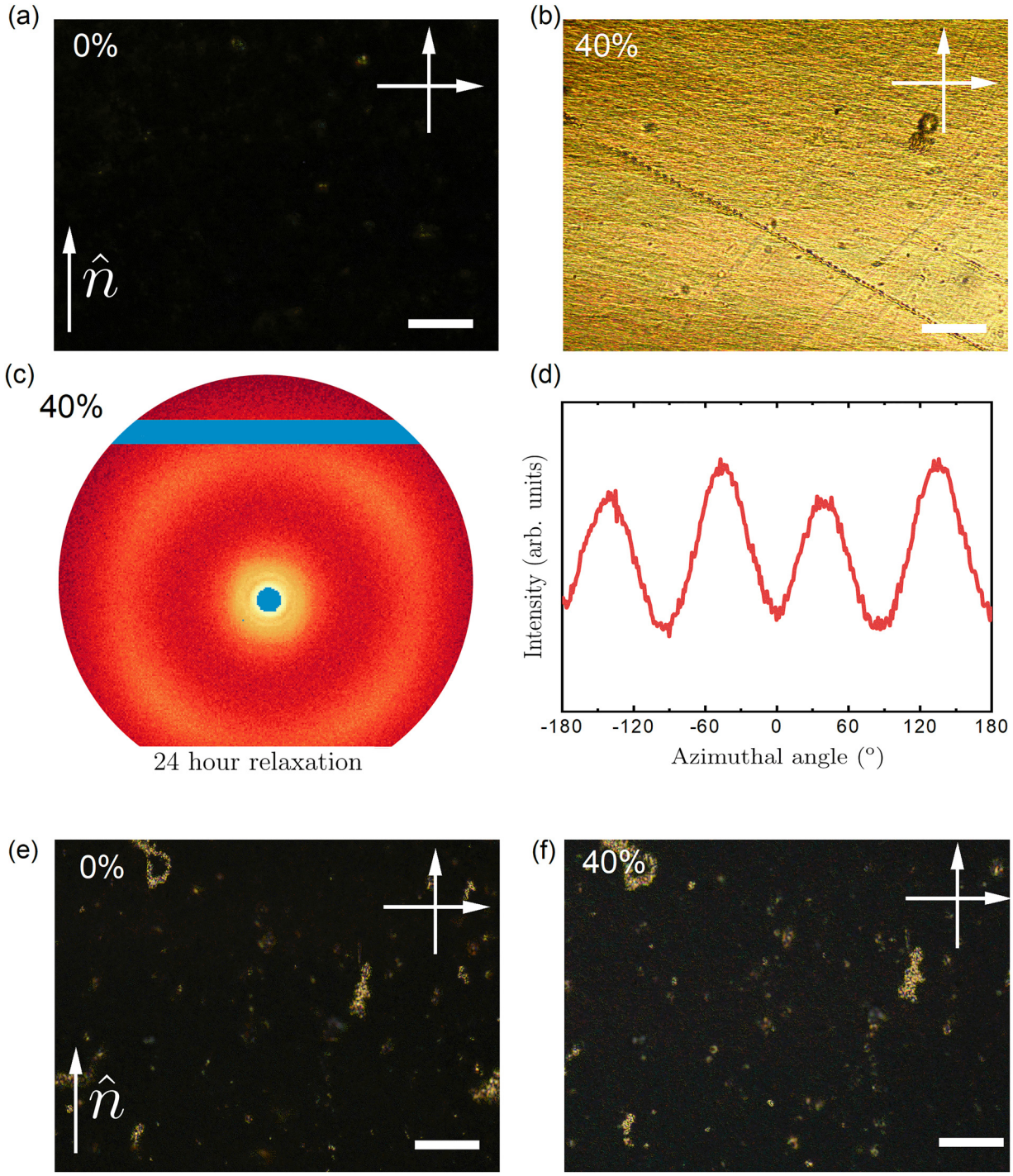

Fig. 8 (a) and (b) Polarised optical microscopy images of the 1× sample at $\varepsilon_{x,true}$ = 0% and $\varepsilon_{x,true}$ = 40% after 24 hours of stress-relaxation, respectively. (c) 2D X-ray scattering image of the 1× sample held at $\varepsilon_{x,true}$ = 40% after 24 hours of stress-relaxation. (d) X-ray scattering profile as a function of azimuthal angle for the 1× sample held at $\varepsilon_{x,true}$ = 50% after 24 hours of stress-relaxation. (e) and (f) Polarised optical microscopy images of the 2× sample at $\varepsilon_{x,true}$ = 0% and $\varepsilon_{x,true}$ = 40% after 24 hours of stress-relaxation, respectively. The arrows in (a), (b), (e) and (f) show the direction of the polariser and analyser, $\hat{n}$ defines the orientation of the director in the unstrained sample. Scale bar = 75 μm.

Discussion

The measurements in the previous section demonstrate clearly that these LCEs deform with characteristics of both SSE and auxetic responses, with the auxetic responses prevalent in the higher cross-link density materials and SSE responses more obvious in the low cross-link density ones. They also show that the dynamics of the system are important in determining which response is observed.

We now consider the underlying reasons why some LCEs exhibit a uniaxial SSE response while others deform biaxially

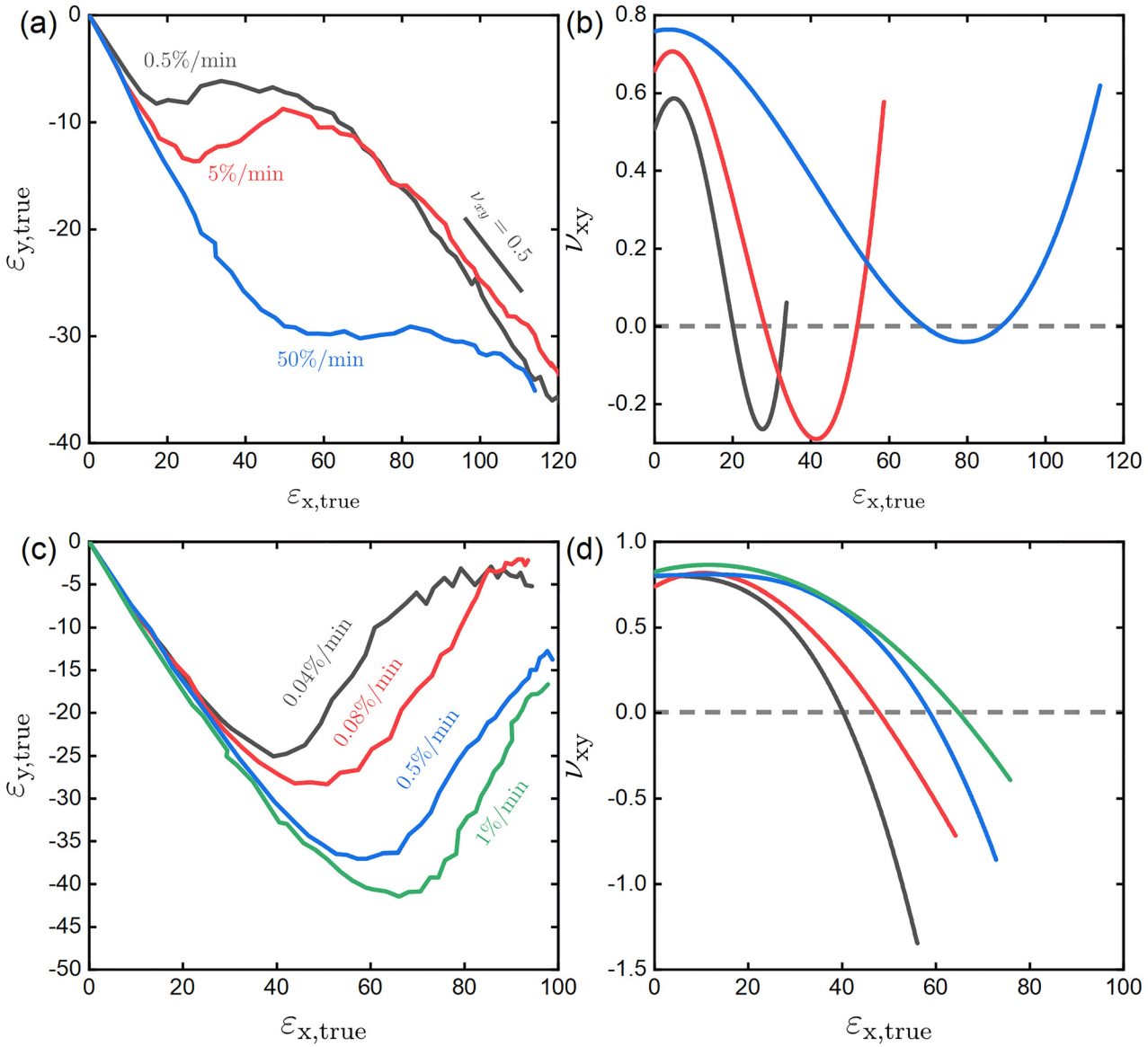

Fig. 9 (a) True strain (ε_y) in the y direction *vs.* true strain (ε_x) in the x direction for the 1/8× sample at strain rates of 0.5% min^{-1} (black), 5% min^{-1} (red) and 50% min^{-1} (blue). (b) Instantaneous x–y Poisson's ratio (ν_{xy}) *vs.* true strain (ε_x) in the x direction for the 1/8× sample at strain rates of 0.5% min^{-1} (black), 5% min^{-1} (red) and 50% min^{-1} (blue). (c) True strain (ε_y) in the y direction *vs.* true strain (ε_x) in the x direction for the 1× samples at strain rates of 0.04% min^{-1} (black), 0.08% min^{-1} (red), 0.5% min^{-1} (blue) and 1% min^{-1} (green). (d) Instantaneous x–y Poisson's ratio (ν_{xy}) *vs.* true strain (ε_x) in the x direction for the 1× sample at strain rates of 0.04% min^{-1} (black), 0.08% min^{-1} (red), 0.5% min^{-1} (blue) and 1% min^{-1} (green). All samples are recorded at T = 23 °C.

and display auxeticity. Previously, it has been suggested that materials displaying an auxetic response must also develop significant biaxiality and theoretical arguments have been provided suggesting that such a response might be enhanced when the measurement temperature is significantly below T_{NI} of the material.[7,51,52] Indeed this work has shown that the samples with larger cross-link density, which also have higher T_{NI}, display larger auxetic responses in both magnitude and in the threshold strain values for a given strain rate. However, this work has also shown that the SSE and auxetic responses can be somewhat mixed, to the extent that the same material can exhibit both behaviours. To gain a deeper insight into that observation, we return to the results of the modified Maier–Saupe model presented earlier. We demonstrated that the LCE with 1× cross-link density had an internal stress field some 3 to 4 times larger than the 1/8× system. Such behaviour is in good agreement with qualitative observations in the literature,[22,37,53] with numerous reports that increased cross-link density increases the criticality of the nematic-to-isotropic transition, broadening it out and increasing T_{NI}. Interestingly, the theoretical arguments that consider the mechanical behaviour of LCEs when supercriticality is present have been discussed. It is suggested that semi-soft elasticity can still occur in supercritical systems, through biaxial phases which spontaneously break symmetry provided that the aligning internal field is small and the measurement is performed close to T_{NI}.[27–29] Here

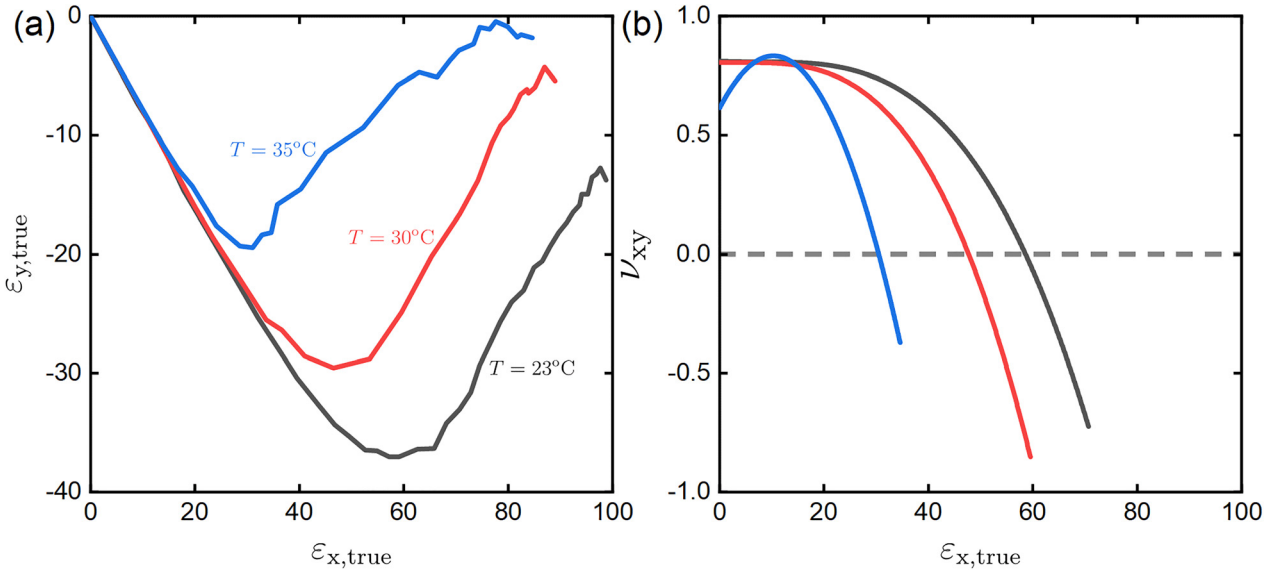

Fig. 10 (a) True strain (ε_y) in the y direction *vs.* true strain (ε_x) in the x direction for the 1× sample at strain rates of 0.5% min^{-1} at T = 23 °C (black), T = 30 °C (red), (c) T = 35 °C (blue). (b) Instantaneous x–y Poisson's ratio (ν_{xy}) *vs.* true strain (ε_x) in the x direction for the 1× sample at a strain rate of 0.5% min^{-1} at T = 23 °C (black), T = 30 °C (red), (c) T = 35 °C (blue).

we find that lower cross-link density LCEs, which have smaller internal strains and for which T_{NI} is significantly closer to the measurement temperature, have only a small biaxial response and in fact display more SSE-like behaviour. The higher cross-linked systems have both high T_{NI} and a high internal stress-field, so the biaxial response is to be expected.

The director behaviour of low cross-link density LCEs was confirmed *via* POM and WAXS to be consistent with that of SSE whereby the director rotates continuously after a threshold strain is reached and there is the formation of stripe domains. The theoretical descriptions of SSE behaviour are extensive and in general the order parameter is assumed to remain constant throughout the deformation[2,3,54] which is consistent with experimental findings of order parameter, which show only a slight increase in the order parameter within the striped domains.[1,48] Such behaviour is markedly different to what is observed in auxetic LCEs which show large reduction in uniaxial order parameters and the emergence of biaxiality.[7,8] A more general theoretical model, encapsulating changes in order, demonstrates that shear striping or auxeticity can be found from the same underlying framework by either constraining order parameters to be constant (shear-stripe case) or allowing uniaxiality to decrease and biaxiality to emerge (auxeticity).[55] Additionally, it suggests the importance of changes in uniaxial order and the emergence of biaxiality in the auxetic response, a result which is paralleled by experiment.[7] Interestingly, the 1/8× RM82 sample which demonstrates clear evidence of classical SSE behaviour, namely a soft-plateau (Fig. 5b), a continuous director rotation (Fig. 6a) and stripe domains (Fig. 6b, d and f) shows evidence of an auxetic response for small strain values (Fig. 5c and d). This may suggest that even for the low cross-link density LCEs, there is some reduction in the order parameter and an emergence of biaxiality which allows for auxeticity to occur before a director rotation at sufficiently small strain rates. This observation has yet to be explored theoretically for conventional SSE behaviour which explicitly constrains the order parameters.

The 1× LCE, shows a clear auxetic response, but after 24 h of relaxation also shows evidence of stripe domains. Additionally, it is found that slower strain rates (and higher temperatures) result in a lower auxetic threshold strain. The latter observation is consistent with findings that show a T_g dependence of the threshold strain in a series of auxetic LCEs with different spacer lengths attaching the mesogenic moieties.[17] Additionally, we find that increasing cross-link density increases the auxetic threshold and magnitude of the auxetic response for LCEs, including those deforming predominantly with an SSE-like characteristic, up till the highest cross-link density (14.8 mol% RM82). Based on these findings we suggest that in these systems SSE and auxeticity is a continuum behaviour dependent on the dynamics of the LCE. It would appear that auxeticity will occur in these LCEs provided that the (i) nematic ordering is robust enough (*i.e.* far from T_{NI}) and the nematic coupling is strong enough to impart an significant internal stress field on the LCE, and (ii) the T_g of the LCE is far enough from the measurement temperature to ensure there is sufficient flexibility to allow for large enough strains to be induced in the LCE whilst also being close enough to the measurement temperature to ensure that the dynamics of the LCE are sufficiently slow, such that relaxation does not occur to the point in which stripe domain formation occurs. Thus, we suggest that the largest auxetic responses will be seen within a dynamic window specific to the material properties.

Conclusions

In this work, we have synthesised a series of LCEs with systematically varied cross-link density and examined their physical

properties in some detail, summarised as follows. The order parameter of the LCE is dependent primarily on the proximity of the curing temperature to the $T_{NI,p}$ of the precursor mixture, as has been reported previously, seen here also as a correlation to the cross-link density.[14] The nematic-to-isotropic transition of the nematic LCEs both increases in temperature and broadens with cross-link density, the latter making it increasingly difficult to observe *via* DSC or POM. Indeed, in the highest cross-link density LCE, T_{NI} could not be observed up to the maximum measurement temperature of 250 °C. A modified Maier–Saupe model was developed and fit to the temperature-dependent order parameter data, revealing that the larger cross-link density LCEs have significant internal stresses with the internal stress field ~3.3 times greater in the 1× LCE (8 mol% RM82) than the 1/8× LCE (1.1 mol% RM82).

The mechanical behaviour of the LCEs was investigated through stress–strain and strain–strain measurements. In all cases except the lowest (0.5 mol% RM82) and the highest cross-link density (14.8 mol% RM82), an ''S''-like characteristic in the stress–strain curve which is associated with either SSE-like behaviour or hyperelasticity was observed. Interestingly, all but the 1/16× LCEs showed evidence of auxeticity, which is not expected for LCEs deforming *via* an SSE response. The director behaviour of the 1/8× and 1× LCEs were investigated *via* POM and WAXS. At a strain rate of 0.1% min^{-1} the 1/8× LCE was confirmed to deform *via* an SSE response through the continuous rotation of the nematic director and the occurrence of stripe domains. The 1× LCE was confirmed to deform in a manner consistent with auxetic LCEs, namely a sharp in-plane director rotation at relatively high strain whilst maintaining optical clarity (no stripe domains). Interestingly, after a 24 h relaxation period at a strain comparable to the auxetic threshold, the 1× LCE displayed stripes domains as evidenced *via* POM and WAXS. The 2× LCE did not display any SSE nature on even a very long timescale. Based on these findings we suggest that SSE and auxetic behaviour are extreme cases on a continuum behaviour which is dependent on the dynamics of the system. We suggest that where T_{NI} is close to the deformation temperature, the LCEs deform primarily *via* the SSE response though an auxetic response may be seen small strains under suitable conditions (temperature and/or strain rate) possibly as a consequence of small changes in order parameter. We further suggest that auxeticity is observed in LCEs provided that the nematic ordering is robust enough (*i.e.* far from T_{NI}) and the nematic coupling is strong enough to impart a significant internal stress field on the LCE. Indeed, theoretical work by Finkelmann *et al.*[52] discussed in detail the mechanical responses of LCEs dependent on the proximity of T_{NI}, revealing that LCEs strained at temperatures much lower than T_{NI} have a lower biaxial stiffnesses relative to uniaxial stiffnesses and are therefore more likely to deform biaxially; a behaviour which is important in the auxetic response.[7] Theoretical work by the Lubensky group discussed in detail the role of the internal stress field on the mechanical response of LCEs revealing that semi-softness can exist deep within the supercritical regime.[27–29] Both of these points are consistent with the findings herein, however it is important to note that all LCEs studied showed some level of auxeticity except for the 1/16× LCE. This point leads us to the importance of the dynamics in the auxetic response of an LCE; auxeticity appears when T_g of the LCE is far enough from the measurement temperature to ensure there is sufficient flexibility to allow for large enough strains to be induced in the LCE whilst also being close enough to the measurement temperature to ensure that the dynamics of the LCE are sufficiently slow such that relaxation does not occur to the point in which stripe domain formation occurs.

This paper provides the first example of a clear cross-over in behaviour on LCEs from semi-soft elasticity to auxeticity. We have shown the importance of dynamics in considering the mechanical response of LCEs. We anticipate that our results will motivate new theoretical works in which the SSE response is investigated whilst allowing for distortions in the nematic ordering of the system.

Author contributions

Conceptualisation: T. R., M. R., H. F. G.; data curation: T. R., M. R., E. J. C.; formal analysis: T. R., M. R., E. J. C., J. H., V. R. H. F. G.; funding acquisition: H. F. G.; investigation: T. R., M. R., E. J. C.; methodology: T. R., M. R., E. J. C., J. H., and V. R.; project administration: T. R. and H. F. G., supervision: H. F. G., validation: T. R. and M. R., visualisation: T. R. and M. R., writing – original draft preparation: T. R. and M. R.; writing – review and editing: T. R., M. R., E. J. C., J. H., V. R., and H. F. G.

Conflicts of interest

H. F. G. holds a position on the board of Auxetec Ltd (Company number 12925662).

Data availability

Supplementary information (SI) is available. See DOI: **https://doi.org/10.1039/d5sm00677e**.

The data underlying this study are openly available at: T. Raistrick, M. Reynolds, E. J. Cooper, J. Hobbs, V. Reshetnyak and H. F. Gleeson, (2025): Dataset associated with ''Resolving the mechanical response of liquid crystal elastomers – semi-soft elastic or auxetic''. University of Leeds. Dataset, **https://doi.org/10.5518/1714**.

Acknowledgements

The authors would like to acknowledge funding from the Engineering and Physical Sciences Research Council, Grant Number EP/V054724/1 and EP/T517860/1. We would also like to acknowledge grant number EP/X0348011 for the purchase of the SAXS/WAXS system used in this work.

References

1 I. Kundler and H. Finkelmann, *Macromol. Rapid Commun.*, 1995, **16**, 679–686.
2 M. Warner and E. M. Terentjev, *Liquid Crystal Elastomers*, Oxford University Press, Oxford, UK, 2007.
3 G. C. Verwey and M. Warner, *Macromolecules*, 1997, **30**, 4189–4195.
4 H. Finkelmann, I. Kundler, E. M. Terentjev and M. Warner, *J. Phys. II*, 1997, **7**, 1059–1069.
5 L. A. Mihai and A. Goriely, *MRS Bull.*, 2021, **46**, 784–794.
6 D. Mistry, S. D. Connell, S. L. Mickthwaite, P. B. Morgan, J. H. Clamp and H. F. Gleeson, *Nat. Commun.*, 2018, **9**, 5095.
7 T. Raistrick, Z. Zhang, D. Mistry, J. Mattsson and H. F. Gleeson, *Phys. Rev. Res.*, 2021, **3**, 023191.
8 Z. Wang, T. Raistrick, A. Street, M. Reynolds, Y. Liu and H. F. Gleeson, *Materials*, 2022, **16**(1), 393.
9 S. R. Berrow, R. J. Mandle, T. Raistrick, M. Reynolds and H. F. Gleeson, *Macromolecules*, 2024, **57**, 5218–5229.
10 P. M. S. Roberts, G. R. Mitchell and F. J. Davis, *J. Phys. II*, 1997, **7**, 1337–1351.
11 M. Liu and Y. Zhao, *Macromolecules*, 2025, **58**(2), 905–918.
12 D. Mistry, P. B. Morgan, J. H. Clamp and H. F. Gleeson, *Soft Matter*, 2018, **14**, 1301–1310.
13 N. Mahardika, T. Raistrick, L. A. Mihai and H. Wang, *Int. J. Solids Struct.*, 2024, **291**, 112717.
14 E. J. Cooper, M. Reynolds, T. Raistrick, S. R. Berrow, E. I. L. Jull, V. Reshetnyak, D. Mistry and H. F. Gleeson, *Macromolecules*, 2024, **57**, 2030–2038.
15 R. Lakes, *Science*, 1987, **235**, 1038–1040.
16 X. Ren, R. Das, P. Tran, T. D. Ngo and Y. M. Xie, *Smart Mater. Struct.*, 2018, **27**, 023001.
17 S. R. Berrow, T. Raistrick, R. J. Mandle and H. F. Gleeson, *Polymers*, 2024, **16**(14), 1957.
18 T. Raistrick, M. Reynolds, H. F. Gleeson and J. Mattsson, *Molecules*, 2021, **26**(23), 7313.
19 T. S. Hebner, C. N. Bowman and T. J. White, *Macromolecules*, 2021, **54**, 4023–4029.
20 M. Barnes, S. Cetinkaya, A. Ajnsztajn and R. Verduzco, *Soft Matter*, 2022, **18**, 5074–5081.
21 P. D. Olmsted, *J. Phys. II*, 1994, **4**, 2215–2230.
22 A. Lebar, G. Cordoyiannis, Z. Kutnjak and B. Zalar, in *Liquid Crystal Elastomers: Materials and Applications*, ed. W. H. de Jeu, Springer Berlin Heidelberg, Berlin, Heidelberg, 2012, pp. 147–185.
23 D. A. Dunmur and P. Palffy-Muhoray, *J. Phys. Chem.*, 1988, **92**, 1406–1419.
24 A. Petelin and M. Čopič, *Phys. Rev. Lett.*, 2009, **103**, 077801.
25 A. Petelin and M. Čopič, *Phys. Rev. E: Stat., Nonlinear, Soft Matter Phys.*, 2010, **82**, 011703.
26 D. Rogez, G. Francius, H. Finkelmann and P. Martinoty, *Eur. Phys. J. E:Soft Matter Biol. Phys.*, 2006, **20**, 369–378.
27 F. Ye, R. Mukhopadhyay, O. Stenull and T. C. Lubensky, *Phys. Rev. Lett.*, 2007, **98**, 147801.
28 F. Ye and T. C. Lubensky, *J. Phys. Chem. B*, 2009, **113**, 3853–3872.
29 T. C. Lubensky and O. Stenull, *Cross-Linked Liquid Crystalline Systems: From Rigid Polymer Networks to Elastomers*, CRC Press, 1st edn, 2011, pp. 381–424.
30 T. Moorhouse and T. Raistrick, *Adv. Opt. Mater.*, 2024, **12**, 2400866.
31 K. Urayama, Y. O. Arai and T. Takigawa, *Macromolecules*, 2005, **38**, 3469–3474.
32 A. Hensel, J. Dobbertin, J. E. K. Schawe, A. Boller and C. Schick, *J. Therm. Anal. Calorim.*, 2005, **46**, 935–954.
33 E. Hempel, G. Hempel, A. Hensel, C. Schick and E. Donth, *J. Phys. Chem. B*, 2000, **104**, 2460–2466.
34 J. C. Dyre, *Rev. Mod. Phys.*, 2006, **78**, 953–972.
35 Z. Zhang and H. F. Gleeson, *Liq. Cryst.*, 2019, **46**, 219–233.
36 T. Raistrick, R. J. Mandle, Z. Zhang, P. J. Tipping and H. F. Gleeson, *Phys. Rev. E*, 2024, **110**, 044702.
37 G. Cordoyiannis, A. Lebar, B. Rožič, B. Zalar, Z. Kutnjak, S. Žumer, F. Brömmel, S. Krause and H. Finkelmann, *Macromolecules*, 2009, **42**, 2069–2073.
38 K. L. Lewis, A. T. Phillips, S. S. Aye, J. C. Chen, J. D. Hoang and T. J. White, *Macromolecules*, 2025, **58**(2), 931–941.
39 J. Schätzle, W. Kaufhold and H. Finkelmann, *Macromol. Chem. Phys.*, 1989, **190**, 3269–3284.
40 J. V. Selinger, H. G. Jeon and B. R. Ratna, *Phys. Rev. Lett.*, 2002, **89**, 225701.
41 P. G. De Gennes, *C. R. Seances Acad. Sci., Ser. B*, 1975, **281**, 101–103.
42 W. Maier and A. Saupe, *Z. Naturforsch., A*, 1958, **13**, 564–566.
43 M. J. Stephen and J. P. Straley, *Rev. Mod. Phys.*, 1974, **46**, 617–704.
44 A. Hotta and E. M. Terentjev, *J. Phys.: Condens. Matter*, 2001, **13**, 11453.
45 T. Ohzono, H. Minamikawa, E. Koyama and Y. Norikane, *Adv. Mater. Interfaces*, 2021, **8**, 2100672.
46 T. Ohzono and E. Koyama, *Polym. Chem.*, 2022, **13**, 2694–2704.
47 *Polymer physics*, ed. M. Rubinstein and R. Colby, Oxford University Press, Oxford, UK, 2003.
48 S. Okamoto, S. Sakurai and K. Urayama, *Soft Matter*, 2021, **17**, 3128–3136.
49 T. Ohzono, H. Minamikawa and E. M. Terentjev, *Commun. Mater.*, 2022, **3**, 29.
50 D. J. Plazek, *J. Rheol.*, 1996, **40**, 987–1014.
51 P. Bladon, E. M. Terentjev and M. Warner, *Phys. Rev. E: Stat. Phys., Plasmas, Fluids, Relat. Interdiscip. Top.*, 1993, **47**, R3838–R3840.
52 H. Finkelmann, A. Greve and M. Warner, *Eur. Phys. J. E: Soft Matter Biol. Phys.*, 2001, **5**, 281–293.
53 G. Cordoyiannis, A. Lebar, B. Zalar, S. Žumer, H. Finkelmann and Z. Kutnjak, *Phys. Rev. Lett.*, 2007, **99**, 197801.
54 A. M. Menzel, H. Pleiner and H. R. Brand, *J. Appl. Phys.*, 2009, **105**, 013503.
55 L. A. Mihai, T. Raistrick, H. F. Gleeson, D. Mistry and A. Goriely, *Liq. Cryst.*, 2023, **50**, 1426–1438.

